Carbohydrate Polymers 83 (2011) 776–786

Contents lists available at ScienceDirect

Carbohydrate Polymers

journal homepage: www.elsevier.com/locate/carbpol

Biodegradable and thermo-sensitive chitosan-*g*-poly(*N*-vinylcaprolactam) nanoparticles as a 5-fluorouracil carrier

N. Sanoj Rejinold [a], K.P. Chennazhi [a], S.V. Nair [a], H. Tamura [b], R. Jayakumar [a,*]

[a] *Amrita Centre for Nanosciences and Molecular Medicine, Amrita Institute of Medical Sciences and Research Centre, Amrita Vishwa Vidyapeetham University, Kochi 682041, India*
[b] *Faculty of Chemistry, Materials and Bioengineering, Kansai University, Osaka 564-8680, Japan*

ARTICLE INFO

Article history:
Received 29 July 2010
Received in revised form 3 August 2010
Accepted 22 August 2010
Available online 27 August 2010

Keywords:
Thermo-responsive graft co-polymeric nanoparticles
LCST
Biomaterials
Cancer drug delivery

ABSTRACT

We developed a nanoformulation of 5-FU (5-fluorouracil) with biodegradable thermo-responsive chitosan-*g*-poly(*N*-vinylcaprolactam) biopolymer composite for its delivery to cancer cells. The novel thermo-responsive graft co-polymeric nanoparticles (TRC-NPs) were prepared by ionic cross-linking method, which showed a lower critical solution temperature (LCST) at 38 °C. The 5-FU drug was incorporated into the carrier using cross-linking reaction. The *in vitro* drug release showed prominent release above LCST. Cytotoxicity assay showed TRC-NPs in the concentration range of 100–1000 μg/ml are non-toxic to an array of cell lines. The drug-loaded nanoparticles showed comparatively higher toxicity to cancer cells while they are less toxic to normal cells. The cell uptake of the 5-FU loaded thermo-responsive graft co-polymeric nanoparticles (5-FU–TRC-NPs) was confirmed from green fluorescence inside cells by rhodamine-123 conjugation. The apoptosis assay showed increased apoptosis of cancer cells when treated with 5-FU compared to the normal cells. These results indicated that novel 5-FU–TRC-NPs could be a promising candidate for cancer drug delivery.

1. Introduction

An exciting potential solution in cancer treatments is to encapsulate the drug in a thermo-responsive biocompatible material that can be injected into the blood stream with the intention of delivering drug to a tumor site in response to an external thermal activation source (Jun, Bochu, & Peng, 2008; Partridge, Burstein, & Winer, 2001; Shapiro & Recht, 2008). Chitin and chitosan are biocompatible, biodegradable and non-toxic polymers (Jayakumar, Nagahama, Furuike, & Tamura, 2008a; Jayakumar, Selvamurugan, Nair, Tokura, & Tamura, 2008b; Jayakumar & Tamura, 2008c; Jayakumar et al., 2009, 2010a; Peter et al., 2009). Because of these properties, it has many applications in tissue engineering (Madhumathi et al., 2009; Maeda, Jayakumar, Nagahama, Furuike, & Tamura, 2008; Nagahama et al., 2008; Peter et al., 2010; Shalumon et al., 2009), wound healing (Sudheesh Kumar et al., 2010), drug delivery (Dev et al., 2010; Manjusha et al., 2010; Muzzarelli, 1988; Thanou, Verhoef, & Junginger, 2001) and also in gene delivery (Anitha et al., 2009; Calvo, Remunan-Lopez, Vila-Jato, & Alonso, 1997a; Calvo, Remunan-Lopez, Vila-Jato, & Alonso, 1997b; Gerrit, 2001; Huang, Khor, & Lim, 2004; Janes & Alonso, 2003; Jayakumar, Prabaharan, Nair, & Tamura, 2010c; Jayakumar et al., 2010d; Richardson, Kolbe, & Duncan, 1999; Vander et al., 2003; Xu & Du, 2003).

In recent years, much interest has been given on water-soluble stimuli responsive polymeric systems that show a phase transition in response to external stimulus such as temperature, pH, specific ion and electric field (Prabaharan, Jamison, Douglas, & Shaoqin, 2008). Among all intelligent polymers studied temperature and pH responsive polymeric systems have drawn more attention, because these are the important physiological factors in the body, and some disease states manifest themselves by a change in either temperature or pH or both. In recent years, several research groups have reported the preparation of pH and temperature sensitive polymers based on the poly(*N*-isopropylacrylamide) (PNIPAAm) for biomedical applications. Poly(*N*-vinylcaprolactam) (PNVCL) is another well studied polymer which shows a well defined response towards temperature as compared to PNIPAAm (Peng & Wu, 2000). The actual interest in PNVCL is connected with its thermo-responsive nature, complexation ability and biocompatibility, both NVCL and its polymer are industrial products that find limited cosmetic applications, and that their safety sheets indicate

Abbreviations: TRC-NPs, thermo-responsive graft co-polymeric nanoparticles; LCST, lower critical solution temperature; LE, loading efficiency; 5-FU–TRC-NPs, 5-FU loaded thermo-responsive graft co-polymeric nanoparticles; NVCL, *N*-vinylcaprolactam; PNVCL, poly(*N*-vinylcaprolactam); PNVCL–COOH, carboxyl terminated poly(*N*-vinylcaprolactam); Chitosan-*g*-PNVCL, chitosan grafted poly(*N*-vinylcaprolactam).

* Corresponding author. Tel.: +91 484 2801234; fax: +91 484 2802020.
E-mail addresses: rjayakumar@aims.amrita.edu, jayakumar77@yahoo.com (R. Jayakumar).

0144-8617/$ – see front matter © 2010 Elsevier Ltd. All rights reserved.
doi:10.1016/j.carbpol.2010.08.052

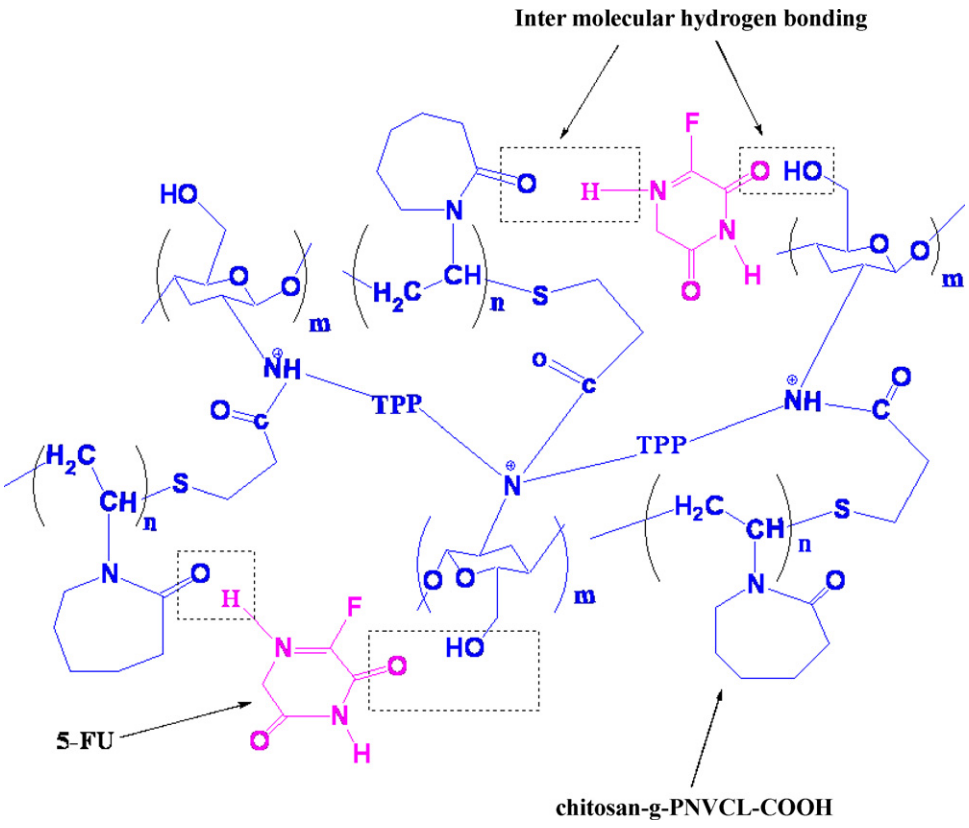

Fig. 1. Loading chemistry for 5-FU in thermo-responsive chitosan-*g*-poly(*N*-vinyl caprolactam) nanoparticles.

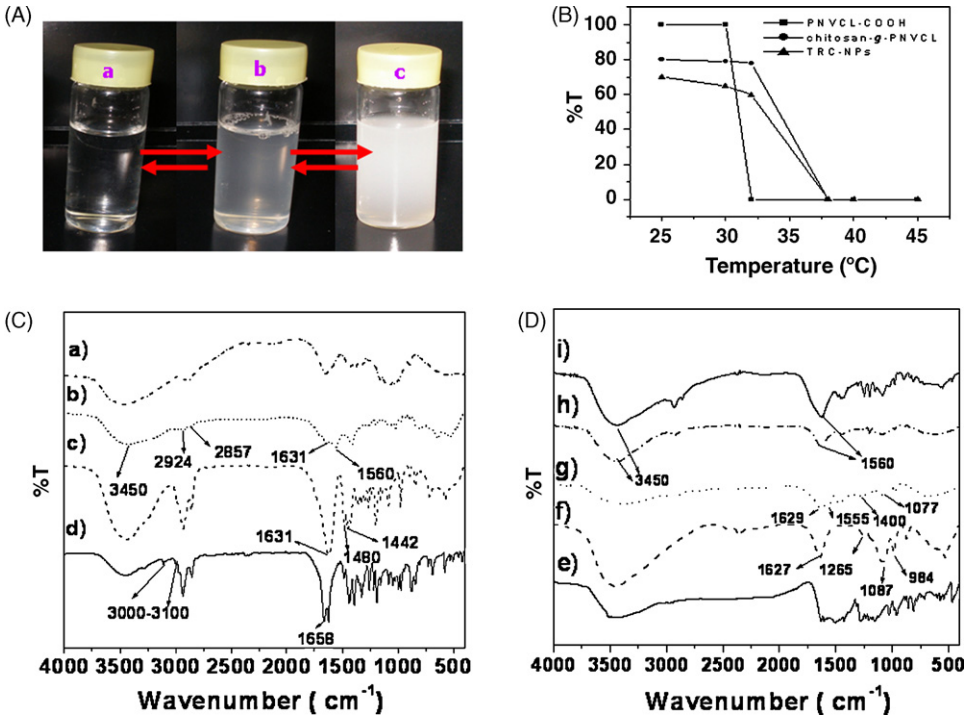

Fig. 2. (A) LCST transitions of chitosan-*g*-poly(*N*-vinylcaprolactam) at different temperatures: (a) at 25 °C, (b) 38 °C and (c) 42 °C. (B) Transmittance (%) analysis of synthesized materials in aqueous solution. (C) FTIR spectrum of (a) chitosan, (b) chitosan-*g*-PNVCL, (c) PNVCL–COOH and (d) monomer NVCL. (D) FTIR spectrum of (e) 5-FU, (f) 5-FU–TRC-NPs, (g) bare TRC-NPs, (h) rhodamine conjugated 5-FU–TRC-NPs and (i) rhodamine conjugated TRC-NPs.

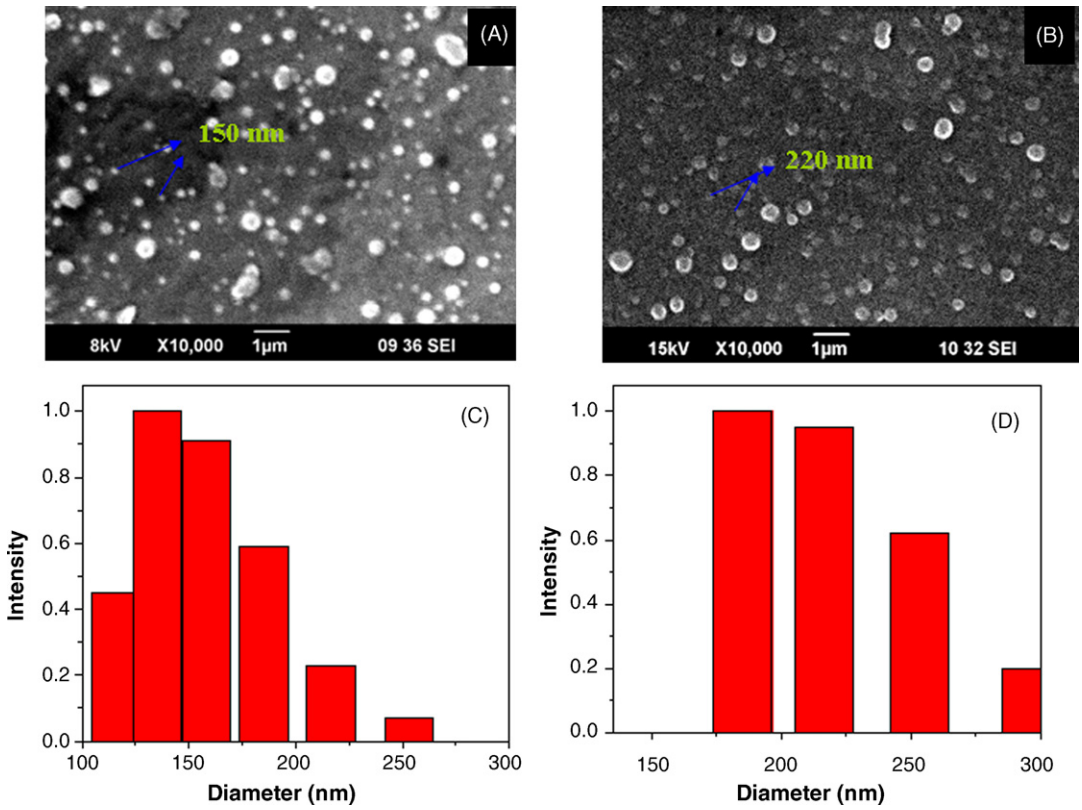

Fig. 3. SEM analysis of (A) TRC–NPs and (B) 5-FU–TRC-NPs; DLS analysis of (C) TRC–NPs and (D) 5-FU–TRC-NPs.

cytotoxicity with a score of 5/10. Presently there are no studies concerning the nanoformulation for cancer drug delivery with these polymers.

5-FU, a pyramidine analogue that interferes with thymidylate synthesis has a broad spectrum of activity against solid tumors (Choi et al., 2007; Kim, Kim, Cho, Yoon, & Song, 2006; Wang, Xiao, Zheng, Chen, & Zou, 2007; Wilkowski, Thoma, Bruns, Wagner, & Heinemann, 2006). Limitations are short biological half-life due to rapid metabolism, incomplete and ununiform oral absorption due to rapid metabolism by dihydropyramidine dehydrogenase and non-selective action against healthy cells. To prolong the circulation time of 5-FU and increase its efficacy, its delivery has to be modified by incorporation into nanoparticulate carriers to reduce the 5-FU associated side effects and thereby improve its therapeutic index.

Hydrophobic drugs like 5-FU rapidly redistribute out of the carrier upon entering the circulation, resulting in pharmacokinetics that are incrementally improved compared to the corresponding free drugs. Highly stable formulations are required to take full advantage of the EPR effect in treating solid tumors (Drummond et al., 2010). Stability is needed for maximizing the duration of exposure and for thermal targeting using hyperthermia to direct the drug-encapsulated thermo-responsive chitosan-*g*-poly(*N*-vinylcaprolactam) nanoparticles to target cancer cells where the drug can then be released locally when the polymer attains its LCST. Nanoscale drug delivery vehicles formulated from biodegradable and biocompatible chitosan and thermo-responsive polymers constitute an evolving approach to drug delivery and tumor targeting. Biodegradable thermo-responsive drug carriers are being purposely engineered and constructed with nanometer dimensions (Jayakumar, Deepthy, Manzoor, Nair, & Tamura, 2010b; Kyung, Jin, Yoon, Jung, & Ki, 2008; Maltzahn et al., 2008). Such approaches make it possible to develop smart materials like thermo-responsive drug delivery vehicles. In this paper we are describing such a smart drug delivery vehicle with an intention of delivering 5-FU only at the tumor site by exploiting the LCST nature of the polymer carrier. The most important advantage of thermo-responsive polymeric nanomaterials includes their high tunability through the switch on and off mechanism and biodegradability since it is conjugated with a biocompatible chitosan moiety. Here we are describing about the nanoformulation, stabilization chemistries, characterization as well as the cytotoxicity, *in vitro* cell uptake and apoptosis studies of 5-FU–TRC-NPs.

2. Experimental

2.1. Synthesis of carboxyl terminated poly(N-vinylcaprolactam) (PNVCL–COOH)

PNVCL–COOH was synthesized by free radical polymerization in isopropanol medium (see supplementary Fig. S1A). Accordingly, *N*-vinylcaprolactam (NVCL) (recrystallized from n hexane before use), mercaptopropionic acid (MPA) and azo bis isobutyronitrile (AIBN) (Sigma–Aldrich) were dissolved in 100 ml of isopropanol (Merk Company Cochin). Dried nitrogen was bubbled into the solution for 15 min prior to polymerization. The reaction was carried out at 75 °C for 6 h under inert atmosphere. After the reaction, the product was precipitated with an excess amount of diethyl ether and dried under vacuum. Thereafter the product was dissolved in 30 ml of millipore water and dialyzed in cellulose membrane tubing (molecular weight cut-off 1000 Da) against distilled water for 3 days to remove the impurities and unreacted materials. Finally the frozen product was lyophilized at −85 °C under 0.085 mbar pressure for further studies.

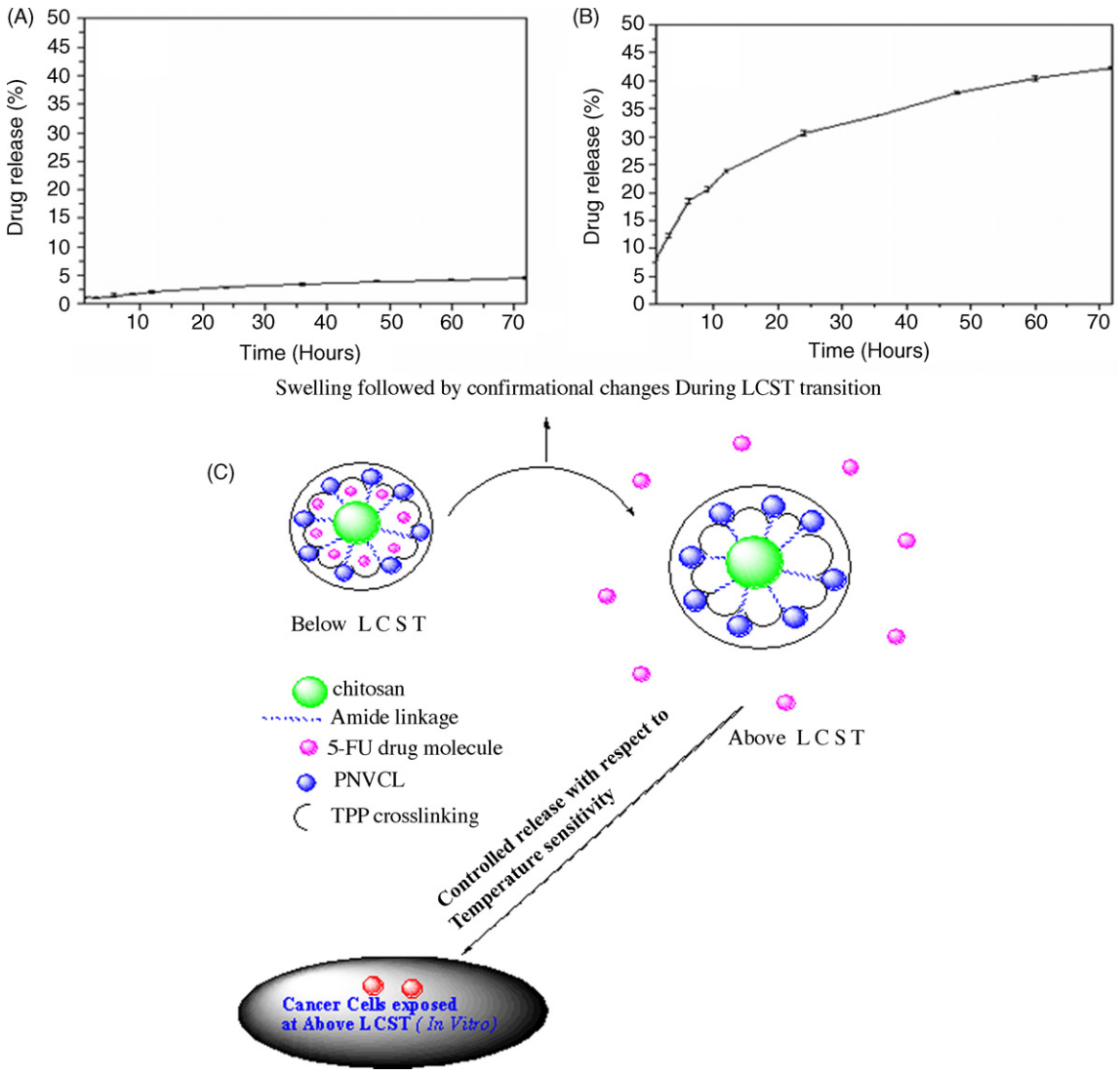

Fig. 4. The drug release profile for the 5-FU from the TRC-NPs above (A) and below (B) LCST (38 °C) and (C) hypothesized mechanism for the controlled release from TRC-NPs.

2.2. Synthesis of chitosan grafted poly(N-vinylcaprolactam) (chitosan-g-PNVCL)

PNVCL–COOH was grafted onto chitosan using (1-ethyl-3-(3-dimethylaminopropyl)carbodiimide/*N*-hydroxy succinimide) EDC/NHS as the condensing agents at room temperature (see supplementary Fig. S1B). First chitosan solution was prepared under uniform stirring in 1% acetic acid. To this, an aqueous solution of PNVCL–COOH (in millipore water) was mixed. Thereafter solution of EDC/NHS (Sigma–Aldrich) (1:2 ratios) in millipore water was added to the reaction mixture drop wise. The reaction was allowed for 12 h at room temperature with constant stirring at low rpm. After dialysis using cellulose membrane tubing (molecular weight cut-off 12 kDa) for 3 days against distilled water, the product was freeze-dried.

2.3. Synthesis of blank TRC-NPs

Chitosan grafted polymer (1:9 ratio polymer) was dissolved in acetic acid (1% solution) and the resulting solution was cross-linked with (sodium tripoly-phosphate) TPP (Sigma–Aldrich) in 1:1 ratio. The resulting nanoformulation was centrifuged at 30,000 rpm for 45 min, resuspended and pelletized several times in water until the pH became 7.4.

2.4. 5-FU loading in TRC-NPs

5-FU–TRC-NPs were prepared by a simple ionic cross-linking method by TPP via aqueous chemistry. Briefly, 5-FU (Sigma–Aldrich) (5 mg in 1 ml water) and polymer (50 mg in 10 ml 1% acetic acid) were stirred for 5 min at low rpm. Further the whole system was mixed with 100 μl TPP solution followed by stirring for 20 min at low rpm. The nanoparticle suspension was then centrifuged at 12,000 rpm for about 45 min and the residue was resuspended in water till the pH become 7.4. The possible loading chemistry is shown in Fig. 1.

2.5. LCST determination

We analyzed LCST of the systems by UV spectrophotometer (Pharma spec) starting from a temperature range of 0–45 °C and an average of three values were taken as the LCST of the synthesized materials.

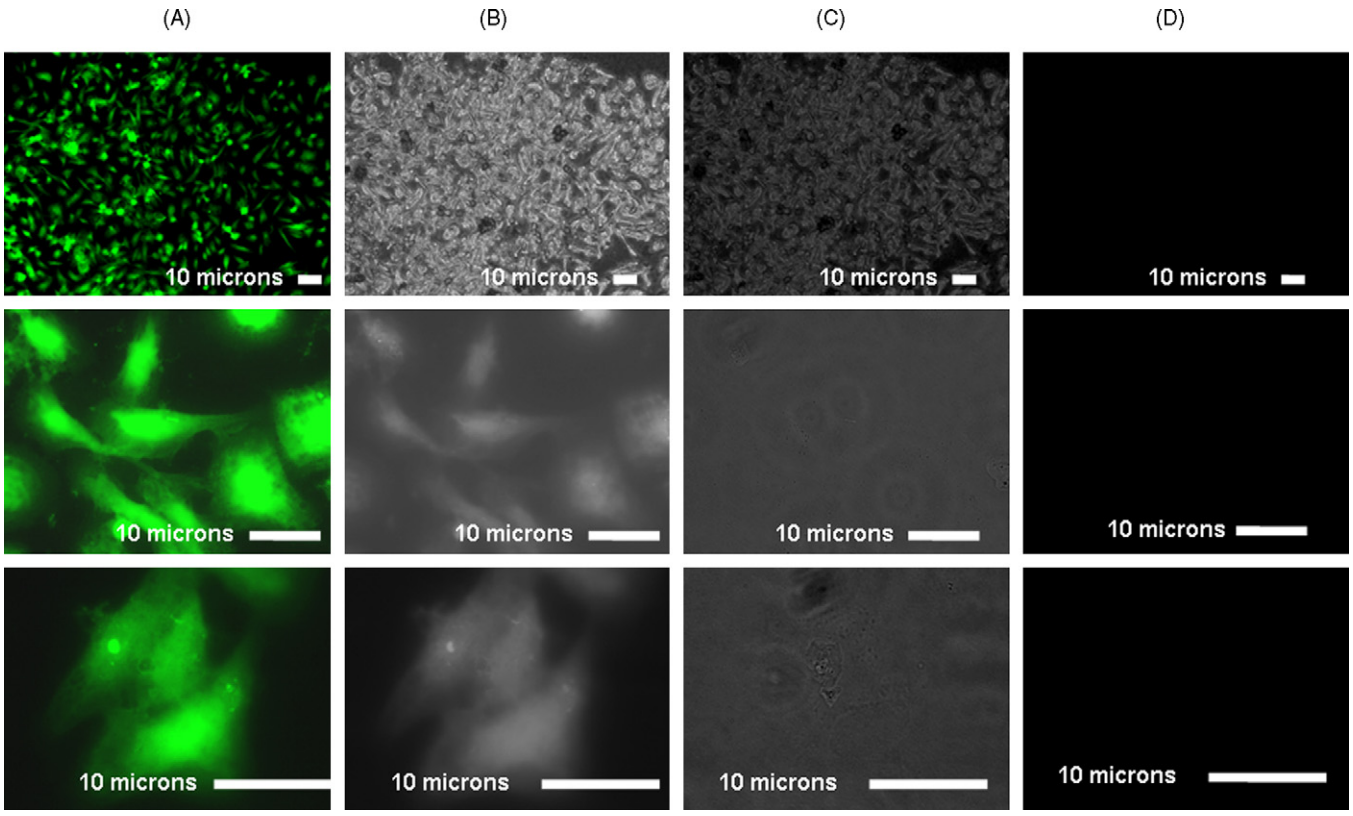

Fig. 5. Fluorescent images showing cellular uptake of rhodamine conjugated 5-FU–TRC-NPs on PC3 (A) display the fluorescence of cells treated with rhodamine conjugated bare TRC-NPs, (B) 5-FU–TRC-NPs and (C) its bright field images, (D) the images of control cells (PC3) with bare TRC-NPs did not show any fluorescence.

2.6. FTIR studies

FTIR spectra of chitosan, monomer *N*-vinylcaprolactam (NVCL), PNVCL–COOH, thermo-responsive chitosan-*g*-PNVCL, TRC-NPs, 5-FU, 5-FU–TRC-NPs were carried out using KBr tablets (1%, w/w of product in KBr) with a resolution of 4 cm^{-1} and 100 scans per sample on a Perkin Elmer Spectrum RX1 apparatus.

2.7. Freeze-drying

In this study, freeze-drying was employed as a means to impart stability or improve shelf life of the developed formulations. Freeze-drying using automated system (*Martin Christ–Lyo Chamber Guard*) was adapted. In brief the conditions were as follows: condenser temperature −85 °C and pressure applied during each step was 0.019 mbar. Two milliliters of the nanoparticle suspension was

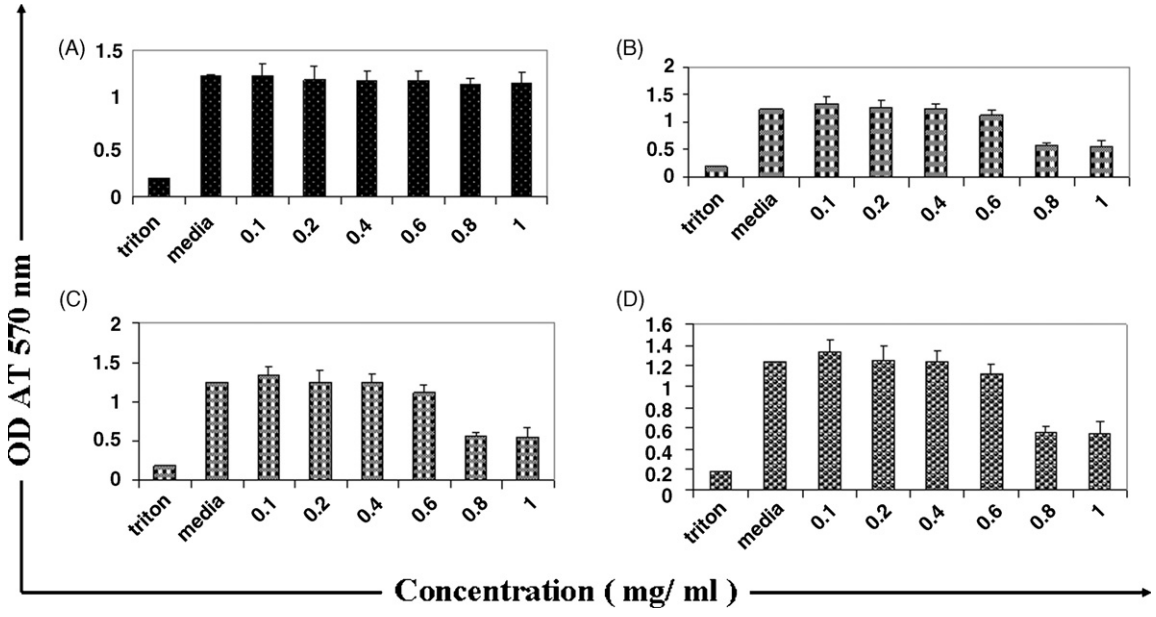

Fig. 6. MTT assay for bare TRC-NPs on (A) L929, (B) PC3, (C) KB and (D) MCF7 after incubated at LCST of the carrier.

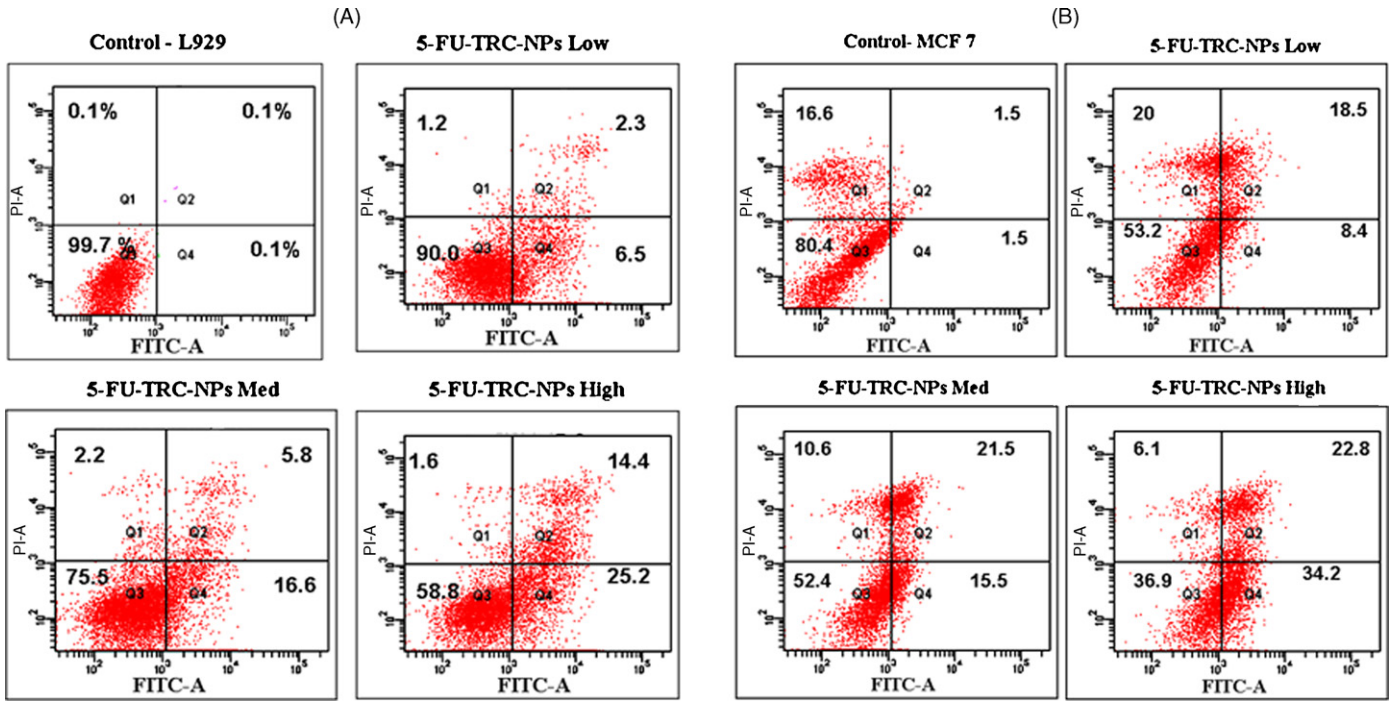

Fig. 7. FACS based apoptosis profile for the 5-FU–TRC-NPs on (A) L929 and (B) MCF7 cells.

filled in 5 ml glass vials. Sucrose 1% (w/v) was added as a cryoprotectant to preserve the particle properties during freezing step. The freeze-dried samples were resuspended in demineralized water and evaluated for size, nature of drug in nanoparticles and morphology.

2.8. Thermal analysis

Thermal studies were done by SII TG/DTA 6200 EXSTAR. The thermal stability and thermal decomposition of prepared systems were investigated using TG/DTA. The temperature scan ranged from 25 °C to 500 °C at a rate of 10 °C/min.

2.9. Nature of drug in nanoparticle (XRD studies)

The patterns of pure 5-FU, TRC-NPs and 5-FU–TRC-NPs were obtained using the X-ray diffractometer (PANalytical X'Pert PRO) with Cu source of radiation. Measurements were performed at voltage of 40 kV and 25 mA. The scanned angle was set from $3^\circ \leq 2\theta \geq 40^\circ$ and the scan rate was $2^\circ\ min^{-1}$.

2.10. Particle size analysis

The particle size was measured by Dynamic light scattering (DLS-ZP/Particle Sizer Nicomp^{TM} 380 ZLS) taking the average of three measurements. The surface morphology of nanoparticle was analyzed by scanning electron microscope (SEM) (JEOLJSM-6490LA). The nanoparticle suspension was placed on the silicon wafer with the help of micropipette tip and allowed to dry overnight in air.

2.11. Loading efficiency (LE)

The percentage of drug incorporated during nanoparticle preparation was determined by centrifuging the drug-loaded nanoparticles at 20,000 rpm for 30 min and separating the supernatant. The supernatant was assayed by UV spectrophotometer (UV-1700 Pharma Spec) at 265 nm by dissolving in ethanol. The calculated LE was 95% using the following formula.

$$\text{Loading efficiency} = \frac{\text{Total amount of 5-FU-Free 5-FU}}{\text{Total amount of 5-FU}} \times 100$$

2.12. In vitro quantification of 5-FU

For *in vitro* quantification of 5-FU, a standard solution of 5-FU was prepared by dissolving 5 mg of 5-FU in 100 ml ethanol solution. A serial dilution from 0.2 to 2 ml was taken and diluted up to 25 ml and assayed at 265 nm using (UV-1700 Pharma Spec) UV spectrophotometer. The data was plotted to get a straight line for the quantification of unknown drug in the nanoparticles.

2.13. In vitro drug release

A known amount of lyophilized TRC-NPs (50 mg) encapsulating 5-FU was dispersed in 10 ml phosphate buffer, pH 7.4, and the solution was divided into 30 eppendorf tubes (500 μl each). The tubes were kept in a thermostable water bath set at two different temperatures (below and above LCST). Free 5-FU is completely soluble in water; therefore at predetermined time intervals the solution was centrifuged at 5000 rpm for 7 min to separate the released 5-FU (which will be in a pellet form) from the loaded TRC-NPs. The released 5-FU was redissolved in 3 ml ethanol to assay spectrophotometrically at 265 nm. The concentration of released drug was then calculated using standard curve of 5-FU in ethanol. The percentage of 5-FU released was determined from the following equation:

$$\text{Release (\%)} = \frac{\text{Released 5-FU from TRC-NPs}}{\text{Total amount of 5-FU in TRC-NPs}} \times 100$$

2.14. Cell culture

MCF 7 (Human Breast cancer cell line, NCCS Pune), L929 (mouse fibroblast cell line, NCCS Pune), KB (oral cancer cell line, NCCS

Pune) were maintained in Minimum Essential Medium (MEM) supplemented with 10% fetal bovine serum (FBS) and PC3 (Prostate Cancer cell lines, NCCS Pune) was maintained in Dulbecco's modified Eagles Medium (DMEM-F12) with 10% FBS. The cells were incubated in an incubator with 5% CO_2. After reaching confluency, the cells were detached from the flask with trypsin–EDTA. The cell suspension was centrifuged at 3000 rpm for 3 min and then resuspended in the growth medium for further studies.

2.15. Cell uptake studies by fluorescence microscopy

Acid etched cover slips kept in 24-well plates were seeded with L929 and PC3 cells with a seeding density of 5000 cells per cover slip and incubated for 24 h for the cells to attach. After the 24 h incubation the media were removed and the wells were carefully washed with PBS buffer. Then the particles at a concentration of 1 mg/ml were added along with the media in triplicate to the wells and incubated for 4 h, thereafter the media with sample were removed and the cover slips were processed for fluorescent microscopy. The processing involved washing the cover slips with PBS and thereafter fixing the cells in 3.7% para-formaldehyde (PFA) followed by a final PBS wash. The cover slips were air dried and mounted on to glass slides with DPX as the mountant medium. The slides were then viewed under the fluorescence microscope (Olympus-BX-51).

2.16. Cytotoxicity studies

For cytotoxicity experiments, L929 (mouse fibroblast cell line, NCCS Pune), MCF7 (Breast cancer cell line, NCCS Pune), PC3 (prostate cancer cell line, NCCS Pune), KB (oral cancer cell line, NCCS Pune) were seeded on a 96-well plate with a density of 10,000 cells/cm^2. MTT [3-(4,5-dimethylthiazole-2-yl)-2,5-diphenyl tetrazolium] assay was used to evaluate cytotoxicity of the prepared nanoparticles and this is a colorimetric test based on the selective ability of viable cells to reduce the tetrazolium component of MTT into purple colored formazan crystals. Five different concentrations of the nanoparticles (0.2 mg/ml, 0.4 mg/ml and 0.6 mg/ml 0.8 mg/ml, 1 mg/ml) were prepared by dilution with the media. After reaching 90% confluency, the cells were washed with PBS buffer and different concentrations of the nanoparticles (100 μl) were added and incubated. Cells in media alone devoid of nanoparticles acted as negative control and wells treated with Triton X-100 as positive control for a period of 24 h. 5 mg of MTT (Sigma) was dissolved in 1 ml of PBS and filter sterilized. 10 μl of the MTT solution was further diluted to 100 μl with 90 μl of serum-free phenol red free medium. The cells were incubated with 100 μl of the above solution for 4 h to form formazan crystals by mitochondrial dehydrogenases. 100 μl of the solubilisation solution (10% Triton X-100, 0.1N HCl and isopropanol) was added in each well and incubated at room temperature for 1 h to dissolve the formazan crystals. The optical density of the solution was measured at a wavelength of 570 nm using a Beckmann Coulter Elisa plate reader (BioTek Power Wave XS). Triplicate samples were analyzed for each experiment.

2.17. Apoptosis assay by flow cytometry (Annexin V-FITC/PI staining)

Phosphatidylserine (PS) translocation from the inner to the outer layer of plasma membrane is one of the important earliest apoptotic features. The PS exposure in both L929 and MCF7 cells was detected using an Annexin V-FITC/PI Vybrant apoptosis assay kit (Molecular probes, Eugene, OR). After reaching 90% confluency the cells were treated with three different concentrations of 5-FU nanoparticles as described previously. After being exposed to 5-FU nanoparticles for 24 h, cells were harvested by trypsinization and washed with ice-cold PBS for 5 min at 500 × g at 4 °C. The supernatant was discarded and the pellet resuspended in ice-cold 1× Annexin binding buffer (5×10^5 to 5×10^6 cells/ml). 5 μl of Annexin V-FITC solution and 1 μl of PI (100 μg/ml) were added to 100 μl of the cell suspensions. The samples were mixed gently and incubated at room temperature for 15 min in the dark. After incubation, 400 μl of ice-cold 1× binding buffer was added and mixed gently, and analyzed by flow cytometry. Cells in media alone devoid of nanoparticles (negative control) and cells treated with bare polymeric nanomaterials were also analyzed in the same way. Triplicate samples were analyzed for each experiment.

2.18. Statistics

Statistical analysis of the data was performed via one-way analysis of variance (ANOVA) using origin software; a value of $p < 0.05$ was considered significant ($n = 3$).

3. Results and discussions

3.1. FTIR studies of polymeric systems and their nanoformulations

The polymerization of NVCL was confirmed by FTIR analysis, characteristic peaks of PNVCL–COOH are located at ν_{max}/cm^{-1} 1631 of amide I band and 1480 νs cm^{-1} (CN), while those of NVCL monomer at 1658 cm^{-1} (C=C) and 3000–3100 cm^{-1} (CH= and CH_2=) disappeared (Fig. 2C (c and d)).

The IR spectra of chitosan and chitosan grafted PNVCL–COOH are shown in Fig. 2A (a and b), respectively. As seen, the spectrum of the graft co-polymer shows not only the characteristic stretching vibration of hydroxyl, aliphatic C–H, and acetylated amino groups from chitosan at 3450, 2922 and 1658 cm^{-1}, respectively, but also the characteristic absorption bands of the amide I band at 1631 and C–N stretching at 2857 cm^{-1}. The newly formed amide bond was confirmed at 1560 cm^{-1}(Laura et al., 2009). The degree of substitution (DS) of PNVCL–COOH onto chitosan was estimated to be ~47%.

In the nanoformulation characteristic peak shift was observed due to the potential interaction of protonated amine/amide groups and negatively charged TPP cross-linking agent. The two possible mechanisms could be (1) TPP interaction with the protonated amide and/or (2) with the protonated amine from the residual chitosan in the grafted polymer (see supplementary Fig. S2A and B). The amine peak at 1630 as shifted to 1629 cm^{-1} due to the interaction with the tripoly-phosphate, and with 5-FU loading the peak again shifted to 1627 cm^{-1}. Similarly there is an amide peak shift from 1560 to 1555 cm^{-1} which is a good evidence for the possibility of TPP-protonated amide interaction as explained before. The wave number shift from higher frequency region to lower frequency region could be attributed to the fact that as TPP cross-linking reaction happened the bond length would have increased, which ultimately would have resulted in the reduction in stretching frequency (stretching frequency and wave number are proportional to each other, $\gamma = c/\lambda$ or $\gamma = c\,\lambda^{-1}$, where λ^{-1} is the wave number) and thereby a shift in wave number as described above (Sanoj Rejinold et al., 2010).

The 5-FU loading and its nanoformulation was confirmed by FTIR analysis by a peak shift in Fig. 2D (e). After 5-FU loading the amine peak of grafted polymer was shifted from 1629 to 1627 cm^{-1} and the amide peak was merged at the same peak. Similarly the peaks at 3450 cm^{-1} seem sharper because of the presence of more F (unbound) groups from the 5-FU. The peaks at 2857–2924 cm^{-1} were also sharper which could be attributed to the presence of more number of C–H groups from the nanopolymeric formulations. The amide peak at 1555 cm^{-1} is vanished, which throws light on the

Table 1
Variation in LCST with respect to polymer concentrations.

Material	Determined LCST
PNVCL–COOH	32 °C
Chitosan-*g*-PNVCL (1:9)	38 °C
Chitosan-*g*-PNVCL (2:8)	41 °C
Chitosan-*g*-PNVCL (3:7)	42 °C
Chitosan-*g*-PNVCL (4:6)	45 °C

fact that 5-FU–TRC-NPs amide interaction in the nanoformulation. Moreover the peaks at 984 and 1087 cm^{-1} (Fig. 2C (f)) confirm the presence of chitosan saccharine residues in nanoformulations.

The rhodamine-123 conjugation on TRC-NPs was confirmed by the sharp peaks at 3450 and 1560 cm^{-1} (Fig. 2D (h and i)) which assures the hydrogen bonding interaction between amine functionalities of rhodamine-123 dye and the OH functionalities from the TRC-NPs.

3.2. LCST analysis of the synthesized materials

The determined LCST of the systems was given in Table 1 and the LCST transition for the grafted polymer in different ratios was also included (Table 1). As seen in Fig. 2A, the chitosan-*g*-PNVCL showed critical solution temperature of 38 °C and below this temperature the system was completely soluble in the water and as temperature increased the density of the particles also increased (Fig. 2A (c)) which could be attributed to reduced hydrogen bonding interaction of the polymer with the water molecules that resulted in hydrogel formation.

The LCST behavior of the bulk system is a reversible process. The most important observation during the analysis was the tunable nature of the LCST which is purely based on the polymer concentration as depicted in Table 1. The enhanced hydrophilic nature of grafted polymer would result in higher LCST as shown in Table 1.

Phase transition temperature is an important parameter for in situ gel-forming polymer, and determines the potential utilization of the polymer in drug delivery (Prabaharan et al., 2008). The LCST of TRC-NPs in aqueous solutions were investigated by measuring the optical transmittance at 480 nm over the temperature range 20–50 °C. There was no phase transition observed for chitosan in the investigated temperature range. Pure PNVCL–COOH and chitosan-*g*-PNVCL co-polymer exhibited phase transition behavior as shown in Fig. 2B. For pure PNVCL–COOH, a LCST at 32 °C was clearly observed. The optical transmittance was almost 100% below 32 °C and it dropped immediately to zero once the temperature was raised above 32 °C. Moreover, the observed LCST of PNVCL–COOH was found to be independent of pH. The reason for the LCST characteristic in thermo-responsive polymers has been well explained in the literature. In the case of PNVCL–COOH, aggregation above the LCST is due to the disruption of hydrogen bonding with water and the increasing hydrophobic interaction among caprolactam groups. For chitosan-*g*-PNVCL co-polymer, its aqueous solution showed a temperature dependent transmittance change due to the introduction of thermo-sensitive PNVCL graft chains, and the LCST value was determined to be 38 °C. The fact that the phase transition temperature of chitosan-*g*-PNVCL was the same as the LCST of pure PNVCL–COOH indicates that aggregation of the grafted PNVCL phase was not affected by the chitosan component.

3.3. Freeze-drying

The 5-FU–TRC-NPs were freeze-dried using sucrose at 5% (w/v), in 3 ml of concentrated nanoparticle suspension (1%, w/v) which resulted in an intact fluffy cake. The hydrodynamic sizes of the lyophilized particles were determined by resuspending in water. The characteristics of the particles before and after 5-FU loading are shown in Fig. 3A–D. The addition of 2 ml of water to the cake (freeze-dried particles) allowed easy resuspension by mere shaking. However, an increase in size was observed.

3.4. Thermal analysis of the synthesized materials

The thermal stability and thermal decomposition of prepared systems were investigated by TG and are given in supplementary Fig. S3A. It shows that the initial degradation temperature of chitosan is very close to 280 °C, slow weight loss starting from 140 to 200 °C due to the decomposition of polymer with low molecular weight, followed by more obvious loss of weight starting from 200 to 310 °C, which could be attributed to a complex process including dehydration of the saccharine rings. The degradation profile of grafted polymer is almost similar to chitosan but less stable compared to chitosan which proves that the system is of amorphous nature. The carboxyl terminated PNVCL has higher stability compared to the chitosan (control). 5-FU degradation nature has been determined to compare the same with loaded TRC-NPs. As per the TG data, the blank TRC-NPs shows slower degradation rate compared to the 5-FU–TRC-NPs which could be due to the more amorphous nature of the 5-FU–TRC-NPs system.

Similarly, the differential thermal analysis of all the systems was preformed to understand the effect of temperature on the behavior of the chitosan, grafted chitosan, 5-FU, TRC-NPs and 5-FU–TRC-NPs. Polysaccharides usually have a strong affinity for water and in solid state these macromolecules may have disordered structures that can be easily hydrated. The hydration properties of polysaccharides depend on primary and supramolecular structures. The endotherm related to evaporation of water is expected to reflect the molecular changes brought in after cross-linking. Thus, chitosan and grafted chitosan had different water-holding capacities. In chitosan the bound water molecules are associated with hydrophilic hydroxyl groups. The thermogram of chitosan showed endotherm at 100 °C (Devika & Varsha, 2006; Radhakumary, Nair, Suresh, & Nair, 2005).

The heat capacity of grafted chitosan with TPP, i.e. (TRC-NPs) was found to be less compared with that of chitosan and chitosan-*g*-PNVCL. The cross-linking reaction via TPP modifies the crystalline nature of chitosan and also the grafted chitosan moiety. The DTA analysis showed 5-FU had started to melt at 180 °C wherein the loaded TRC-NPs, the same endotherm peak was shifted to 150 °C which assures the amorphous nature of the 5-FU–TRC-NPs (see supplementary Fig. S3B).

On the basis of these results it can be stated that increase in the polar groups and reduction in crystalline domains caused reduction in heat capacity/thermal stability. The second thermal event observed was the presence of exotherms due to the decomposition of the polymer. Owing to the differences in the chemical characteristics, changes in the exothermic peak of chitosan and cross-linked chitosan were also observed. Characterization of cross-linked chitosan polymer and its 5-FU loaded nanoparticles were analyzed by XRD and FTIR provided the evidence of reduction in crystallinity after cross-linking with TPP. The TG/DTA analysis confirms the more amorphous nature for the cross-linked TRC-NPs and 5-FU–TRC-NPs.

3.5. Nature of drug in nanoparticles by XRD studies

X-ray analysis was conducted in order to compare 5-FU–TRC-NPs with the bare 5-FU and its nanocarrier. Bare 5-FU is highly crystalline in nature. It has been observed that sharp peaks in their XRD spectra indicating high crystalline nature. TG/DTA also confirmed the same character to 5-FU. The loaded TRC-NPs showed

broader spectrum in the XRD studies (see supplementary Fig. S3C) as blank TRC-NPs. The high amorphous nature could be accounted to the two mechanisms as described in the previous section. The more amorphous the polymeric carrier system, higher would be the release percentage of the loaded drugs (Abdelwahed, Degobert, Stainmesse, & Fessi, 2006; Furqan maulvi, Thakkar, Soni, Gohel, & Gandhi, 2009).

3.6. Particle size and topography

Fig. 3A and B shows the SEM images of the synthesized TRC-NPs, which confirm the TRC-NPs are nearly spherical in shape with an average diameter of 150 nm whereas the 5-FU–TRC-NPs showed a size range of 180–220 nm and the increase in particle size could be attributed to the loading of 5-FU on TRC-NPs. The DLS analysis also confirmed the particles are in the same range described above (Fig. 3C and D).

3.7. In vitro drug release

In vitro drug release was done at two different temperatures (above and below LCST) to evaluate the thermo-responsive nature of the nanoparticle in PBS solution (pH 7.4) for 3 days. Fig. 4A shows the release profile for the 5-FU from the TRC-NPs at above and below the LCST (Fig. 4B) of the carrier system. After 3 days experiment 40% 5-FU has been released above LCST of the system while at below LCST, only a 5% drug release is observed which confirms the drug release mechanism is based on the LCST of the polymeric carrier system. The 5% drug release could be due to the presence of unbound drug onto the surface of the TRC-NPs. There are different factors involved in the complex formation of TRC-NPs with 5-FU that include the van der Waals interaction between the hydrophobic moiety of the drug molecules and the PNVCL side chains, hydrogen bonding between the polar functional groups of drug molecules and the hydroxyl groups of chitosan-*g*-PNVCL.

There are three primary mechanisms by which the release of drug molecules can be controlled: erosion, diffusion, and swelling followed by diffusion (Peppas, 1985). Compared to the previous studies on chitosan-*g*-PNVCL as micro-beads (Prabaharan et al., 2008), our nanoformulation showed very controlled and sustained release of 5-FU from the TRC-NPs, which is essential in cancer drug delivery. In TRC-NPs, it was observed that drug release is prominent above LCST in the initial period compared to that below LCST. About 10–20% of the drug has been released within 10 h at above LCST. Thereafter, a much slower and almost constant release rate is observed. It seems that release is influenced by swelling, especially in the initial period of release above LCST. After this initial period, in which the swelling equilibrium is achieved, the release most probably follows diffusion-controlled mechanism. In the initial period, hydration followed by polymer chain relaxation takes place by penetration of water into the matrix. During this process, high release rates occur due to the presence of the drug at and near the surface. After forming the gel structure, the release continues with the diffusion mechanism through the matrix by a much slower release rate. However, the drug release is very slow and almost less than 5% at below LCST which assures that there would not be any change for the above said mechanism. Above LCST the TRC-NPs would lose its hydrogen bonding interaction with 5-FU hence the drug–carrier interaction would be less and carrier–carrier molecules interaction would be high, whereas below LCST hydrogen bonding would be strong enough to hold the drug molecules on it.

3.8. Fluorescence microscopy

Cellular uptake studies of 5-FU–TRC-NPs were done by rhodamine-123 conjugation, and visualizing the dye using fluorescence microscopy. Fig. 5 displays the fluorescent images of rhodamine conjugated 5-FU–TRC-NPs on PC3. The same study on L929 is given in materials section (see supplementary Fig. S4). Images of control cells without any drug and cells incubated with empty TRC-NPs did not show any fluorescence. Because of the internalization of both free and rodamine conjugated 5-FU–TRC-NPs, images of the cells showed green fluorescence.

3.9. Cytotoxicity studies

MTT assay was done for six different concentrations, viz., 0.1–1 mg/ml. Triton X-100 was taken as the positive control for cytotoxicity. Here in our study there is no significant cytotoxicity in any of the concentrations of the bare TRC-NPs studied (see supplementary Fig. S5). Similarly, we also compared the level of toxicity of nanoparticles with the negative control, which are the cells grown in its respective media. It is evident from supplementary Fig. S5 that compared to the negative control almost 98% cells are viable in all the six concentrations of TRC-NPs. These results indicated that the prepared nanoparticle carriers are non-toxic to L929, KB, PC3 and MCF7. The same experiments were analyzed with 5-FU–TRC-NPs in the same concentration range (0.1–1 mg/ml) (Fig. 6) after incubation at 38 °C. From our experimental observations it is evident that the 5-FU–TRC-NPs showed comparatively less toxicity on L929 cells, while specific toxicity has been observed on to PC3, KB and MCF7 cell lines. The results were further confirmed by FACS based apoptosis assay on L929 and MCF cells.

3.10. Apoptosis assay by flow cytometry (Annexin V-FITC/PI staining)

Phosphatidylserine (PS) is exposed during early apoptosis by flipping from the inner to the outer layer of plasma membrane, and Annexin V has the ability to bind to PS with high affinity. Furthermore, propidium iodide (PI) conjugates to necrotic cells. Since Annexin V is conjugated to FITC, double staining with FITC-Annexin V and PI is used to detect apoptosis and necrosis. Four distinct phenotypes were distinguishable: viable (lower left quadrant, Q3), early apoptotic (lower right quadrant, Q4), late apoptotic and necrotic (upper right quadrant, Q2), and damaged cells (upper left quadrant, Q1). The blank TRC-NPs did not show any apoptosis in any of the three concentrations. Necrotic cells have been observed in the case of MCF7 cells, may be due to the dead cells during the experiment.

supplementary Fig. S6 shows the apoptotic profile of bare TRC-NPs and Fig. 7 for 5-FU–TRC-NPs. As seen in Fig. 7, more percentage of apoptotic cells were observed in the case of MCF7 compared to that L929 cell line. We checked three concentrations of 5-FU–TRC-NPs as low (0.2 mg/ml){[5-FU]} = 1.9 μg, medium (0.6 mg/ml) {[5-FU]} = 4.6 μg and a higher concentration as (1 mg/ml) {[5-FU]} = 8.6 μg. A concentration dependent increase in apoptosis is observed in the case of breast cancer cells (MCF7). Our results clearly support the fact that there is differential sensitivity of cell lines to 5-FU–TRC-NPs. Among various factors that are responsible for preferential uptake in tumor cells against normal cells; difference in membrane structure, protein composition and bigger size could be the prime reason.

4. Conclusion

Biodegradable and thermo-responsive polymeric nanoparticles were synthesized and characterized for cancer drug delivery. Due to the presence of PNVCL, chitosan co-polymer showed a temperature-induced phase transition and LCST was determined in the range of 38–45 °C in aqueous solutions. The 5-FU drug release

was found to be more prominent above its LCST temperature compared to that below LCST. The TRC-NPs were non-toxic in the concentration range of 0.1–1.0 mg/ml to normal and cancer cells. The 5-FU–TRC-NPs have shown to be toxic to PC3, KB and MCF7 cancer cells which are further confirmed by the FACS based Apoptosis assay. These results indicated that the 5-FU–TRC-NPs can be used for cancer drug delivery and thus novel 5-FU–TRC-NPs could be more beneficial for cancer treatment when subjected to temperature increase using external sources.

Acknowledgments

The Department of Biotechnology, Government of India supported this work, under a grant of the Nanoscience and Nanotechnology Initiative program (Ref. No. BT/PR10850/NNT/28/127/2008). This work was also partially supported by Department of Science and Technology (DST) under a center grant of the Nanoscience and Nanotechnology Initiative program monitored by Dr. C. N. R. Rao. The authors are also thankful to Mr. Sajin. P. Ravi for his technical support.

Appendix A. Supplementary data

Supplementary data associated with this article can be found, in the online version, at doi:10.1016/j.carbpol.2010.08.052.

References

Abdelwahed, W., Degobert, G., Stainmesse, S., & Fessi, H. (2006). Freeze-drying of nanoparticles: Formulation, process and storage considerations. *Advanced Drug Delivery Revision*, *58*, 1688–1713.

Anitha, A., Divya Rani, V. V., Krishna, R., Sreeja, V., Selvamurugan, N., Nair, S. V., et al. (2009). Synthesis, characterization, cytotoxicity and antibacterial studies of chitosan, *O*-carboxymethyl and *N*, *O*-carboxymethyl chitosan nanoparticles. *Carbohydrate Polymers*, *78*, 672–677.

Calvo, P., Remunan-Lopez, C., Vila-Jato, C. L., & Alonso, M. J. (1997a). Novel hydrophilic chitosan-polyethylene oxide nanoparticles as protein carriers. *Journal of Applied Polymer Science*, *63*, 125–132.

Calvo, P., Remunan-Lopez, C., Vila-Jato, C. L., & Alonso, M. J. (1997b). Chitosan and chitosan/ethylene oxide-propylene oxide block copolymer nanoparticles as novel carriers for proteins and vaccines. *Pharmaceutical Research*, *14*, 1431–1436.

Choi, I. S., Oh, D. Y., Kim, B. S., Lee, K. W., Kim, J. H., & Seok Lee, J. (2007). 5-FU, folinic acid as first-line palliative chemotherapy in elderly patients with metastatic or recurrent gastric cancer. *Cancer Research Treatment*, *39*, 99–103.

Dev, A., Binulal, N. S., Anitha, A., Nair, S. V., Furuike, T., Tamura, H., et al. (2010). Preparation of poly (lactic acid)/chitosan nanoparticles for anti-HIV drug delivery applications. *Carbohydrate Polymers*, *80*, 833–838.

Devika, R. B., & Varsha, P. (2006). Studies on effect of pH on cross-linking of chitosan with sodium tripolyphosphate: A technical note. *AAPS Pharmaceutical Science and Technology*, *7*, E1–E6.

Drummond, D. C., Noble, C. O., Guo, Z., Hayes, M. E., Ingram, C. C., Gabriel, B. S., et al. (2010). Development of a highly stable and targetable nanoliposomal formulation of topotecan. *Journal of Controlled Release*, *141*, 13–21.

Furqan maulvi, V. T. T., Thakkar, V. T., Soni, T. G., Gohel, M. C., & Gandhi, T. R. (2009). Supercritical fluid technology: A promising approach to enhance the drug solubility. *Journal of Pharmaceutical Sciences and Research*, *4*, 1–14.

Gerrit, B. (2001). Chitosans for gene delivery. *Advanced Drug Delivery Revision*, *2*, 145–150.

Huang, M., Khor, E., & Lim, L. Y. (2004). Uptake and Cytotoxicity of chitosan molecules and nanoparticles: Effects of molecular weight and degree of deacetylation. *Pharmaceutical Research*, *21*, 344–353.

Janes, K. A., & Alonso, M. J. (2003). Depolymerized chitosan nanoparticles for protein delivery: Preparation and characterization. *Journal of Applied Polymer Science*, *88*, 2766–2779.

Jayakumar, R., Chennazhi, K. P., Muzzarelli, R. A. A., Tamura, H., Nair, S. V., & Selvamurugan, N. (2010). Chitosan conjugated DNA nanoparticles in gene therapy. *Carbohydrate Polymers*, *79*, 1–8.

Jayakumar, R., Deepthy, M., Manzoor, K., Nair, S. V., & Tamura, H. (2010). Biomedical applications of chitin and chitosan based nanomaterials—A short review. *Carbohydrate Polymers*, doi:10.1016/j.carbpol.2010.04.074

Jayakumar, R., Divya Rani, V. V., Shalumon, K. T., Sudheesh Kumar, P. T., Nair, S. V., Furuike, T., et al. (2009). Bioactive and osteoblast cell attachment studies of novel α-and β-chitin membranes for tissue-engineering applications. *International Journal of Biological Macromolecules*, *45*, 260–264.

Jayakumar, R., Nagahama, H., Furuike, T., & Tamura, H. (2008). Synthesis of phosphorylated chitosan by novel method and its characterization. *International Journal of Biological Macromolecules*, *42*, 335–339.

Jayakumar, R., Prabaharan, M., Nair, S. V., & Tamura, H. (2010). Novel chitin and chitosan nanofibers in biomedical applications. *Biotechnology Advances*, *28*, 142–150.

Jayakumar, R., Prabaharan, M., Nair, S. V., Tokura, S., Tamura, H., & Selvamurugan, N. (2010). Novel carboxymethyl derivatives of chitin and chitosan materials and their biomedical applications. *Progress in Material Sciences*, *55*, 675–709.

Jayakumar, R., Selvamurugan, N., Nair, S. V., Tokura, S., & Tamura, H. (2008). Preparative methods of phosphorylated chitin and chitosan—An overview. *International Journal of Biological Macromolecules*, *43*, 221–225.

Jayakumar, R., & Tamura, H. (2008). Synthesis, characterization and thermal properties of chitin-g-poly (ε-caprolactone) copolymers by using chitin gel. *International Journal of Biological Macromolecules*, *43*, 32–36.

Jun, L., Bochu, W., & Peng, L. (2008). Possibility of active targeting to tumor by local hyperthermia with temperature sensitive nanoparticles. *Medical Hypotheses*, *71*, 249–251.

Kim, J. S., Kim, J. S., Cho, M. J., Yoon, W. H., & Song, K. S. (2006). Comparison of the efficacy of oral capecitabine versus bolus 5-FU in preoperative radiotherapy of locally advanced rectal cancer. *Journal of Korean Medical Sciences*, *21*, 52–57.

Kyung, M. P., Jin, W. B., Yoon, K. J., Jung, W. S., & Ki, D. P. (2008). Nanoaggregate of thermo sensitive chitosan-pluronic for sustained release of hydrophobic drug. *Colloids Surfaces B*, *63*, 1–6.

Laura, B. S., Yanjie, Z., Vladislav, A., Litosh, C., Xin, C., Younhee, et al. (2009). Investigating the hydrogen-bonding model of urea denaturation. *Journal of American Chemical Society*, *131*, 26–31.

Madhumathi, K., Sudheesh Kumar, P. T., Kavya, K. C., Furuike, T., Tamura, H., Nair, S. V., et al. (2009). Novel chitin/nanosilica composite scaffolds for bone tissue engineering applications. *International Journal of Biological Macromolecules*, *45*, 289–292.

Maeda, Y., Jayakumar, R., Nagahama, H., Furuike, T., & Tamura, H. (2008). Synthesis, characterization and bioactivity studies of novel β-chitin scaffolds for tissue-engineering applications. *International Journal of Biological Macromolecules*, *42*, 1463–1467.

Maltzahn, V. G., Ren, Y., Park, J. H., Min, D. H., Kotamraju, V. R., Jayakumar, J., Fogal, V., Sailor, M. J., Ruoslahti, E., & Bhatia, S. N. (2008). In vivo tumor cell targeting with "Click" nanoparticles. *Bioconjugate Chemistry*, *19*, 1570–1578.

Manjusha, E. M., Jithin, C. M., Manzoor, K., Nair, S. V., Tamura, H., & Jayakumar, R. (2010). Folate conjugated carboxymethyl chitosan-manganese doped zinc sulphide nanoparticles for targeted drug delivery and imaging of cancer cells. *Carbohydrate Polymers*, *80*, 442–448.

Muzzarelli, R. A. A. (1988). Carboxymethylated chitin and chitosans. *Carbohydrate Polymers*, *8*, 1–21.

Nagahama, H., New, N., Jayakumar, R., Koiwa, S., Furuike, T., & Tamura, H. (2008). Novel biodegradable chitin membranes for tissue engineering applications. *Carbohydrate Polymers*, *73*, 295–302.

Partridge, A. H., Burstein, H. J., & Winer, E. P. (2001). *Journal of National Cancer Institute Monographs*, *2001*, 135–142.

Peng, S., & Wu, C. (2000). Poly (*N*-vinyl caprolatum) micro gels and its related composites. *Macromolecular Symposium*, *159*, 179–186.

Peppas, N. A. (1985). Analysis of Fickian and non-Fickian drug release from polymers. *Pharmaceutical Acta Helvetiae*, *60*, 110–111.

Peter, M., Binulal, N. S., Nair, S. V., Selvamurugan, N., Tamura, H., & Jayakumar, R. (2010). Novel biodegradable chitosan-gelatin/nano-bioactive glass ceramic composite scaffolds for alveolar bone tissue engineering. *Chemical Engineering Journal*, *158*, 353–361.

Peter, M., Sudheesh Kumar, P. T., Binulal, N. S., Nair, S. V., Tamura, H., & Jayakumar, R. (2009). Development of novel α-chitin/nanobioactive glass ceramic composite scaffolds for tissue engineering applications. *Carbohydrate Polymers*, *78*, 926–931.

Prabaharan, M., Jamison, J., Grailer, Douglas, S. A., & Shaoqin, G. (2008). Stimuli-responsive chitosan-graft-poly (*N*-vinylcaprolactam) as a promising material for controlled hydrophobic drug delivery. *Macromolecular Biosciences*, *8*, 843–851.

Radhakumary, C., Nair, P. D., Suresh, M., & Nair, C. P. R. (2005). Trends in pharmacological sciences. *Trends Biomaterials and Artificial Organs*, *30*, 117–124.

Richardson, C. W., Kolbe, H. V. J., & Duncan, R. (1999). Potential of low molecular mass chitosan as a DNA delivery system: Biocompatibility, body distribution and ability to complex and protect DNA. *International Journal of Pharmacy*, *178*, 231–243.

Sanoj Rejinold, N., Muthunarayanan, M., Deepa, N., Chennazhi, K. P., Nair, S. V., & Jayakumar, R. (2010). Development of novel fibrinogen nanoparticles by two step co-acervation method. *International Journal of Biological Macromolecules*, *47*, 37–43.

Shalumon, K. T., Binulal, N. S., Selvamurugan, N., Nair, S. V., Deepthy Menon, Furuike, T., et al. (2009). Electrospinning of carboxymethyl chitin/poly (vinyl alcohol) nanofibrous scaffolds for tissue engineering applications. *Carbohydrate Polymers*, *77*, 863–869.

Shapiro, C. L., & Recht, A. (2008). Side effects of adjuvant treatment of breast cancer National England. *Journal of Medicine*, *344*, 1997–2001.

Sudheesh Kumar, P. T., Abhilash, S., Manzoor, K., Nair, S. V., Tamura, H., & Jayakumar, R. (2010). Preparation and characterization of novel β-chitin/nanosilver

composite scaffolds for wound dressing applications. *Carbohydrate Polymers*, *80*, 761–767.

Thanou, M., Verhoef, J. C., & Junginger, H. E. (2001). Oral drug absorption enhancement by chitosan and its derivatives. *Advanced Drug Delivery Revision*, *52*, 117–126.

Vander, L. I., Kersten, M. V., Fretz, G., Beuvery, M. M., Verhoef, J. C., & Junginger, H. E. (2003). Chitosan micro particles for mucosal vaccination against diphtheria: Oral and nasal efficacy studies in mice. *Vaccine*, *21*, 1400–1408.

Wang, J. M., Xiao, B. L., Zheng, J. W., Chen, H. B., & Zou, S. Q. (2007). Effect of targeted magnetic nanoparticles containing 5-FU on expression of bcl-2, bax and caspase 3 in nude mice with transplanted human liver cancer. *World Journal of Gastroenterology*, *3*, 3171–3175.

Wilkowski, R., Thoma, M., Bruns, C., Wagner, A., & Heinemann, V. (2006). Chemo radiotherapy with gemcitabine and continuous 5-FU in patients with primary inoperable pancreatic cancer. *Journal of Pancreas*, *7*, 349–360.

Xu, Y., & Du, Y. (2003). Effect of molecular structure of chitosan on protein delivery. *International Journal of Pharmacy*, *250*, 215–226.